Yili Xia, Scott C. Douglas, and Danilo P. Mandic

Adaptive Frequency Estimation in Smart Grid Applications

[Exploiting noncircularity
and widely linear adaptive
estimators]

ISTOCKPHOTO.COM© SIGAL SUHLER MORAN

**Technical Challenges
of the Smart Grid**

ccurate estimation of system frequency in real time is a prerequisite for the future smart grid, where the generation, loading, and topology will all be dynamically updated. In this article, we introduce a unified framework for the estimation of instantaneous frequency in both balanced and unbalanced conditions in a three-phase system, thus consolidating the existing approaches and providing next-generation solutions capable of joint adaptive frequency estimation and system fault identification. This is achieved by employing recent developments in the statistics of complex variables (augmented statistics) and the associated widely linear models, allowing us to benefit from a rigorous account of varying degrees of noncircularity corresponding to different sources of frequency variations. The advantages of such an approach are illustrated for both balanced and unbalanced conditions, including voltage sags, harmonics and supply-demand mismatch, all major obstacles for accurate frequency estimation in the smart grid.

WHY FREQUENCY ESTIMATION IN THE SMART GRID

Electricity networks are undergoing wholesale changes both from the generation and the user (load) sides. Major challenges in this direction are envisaged to be the management of largely increased load levels, due to e.g., charging a large number of plug-in electric vehicles (PEVs), and the duality between loads and supplies, for instance, when PEVs are used in the "vehicle to grid" mode to mitigate power shortage and system imbalances. Generation, historically aggregated into large power plants and far from the user, is gradually moving towards being located at the distribution level and based on renewable sources, that is, intrinsically intermittent [1]. This will require enhanced flexibility of the grid and the ability to accommodate islanding and microgrids [2], [3].

The idea behind smart distributed grids and microgrids is to balance as much as possible locally between production and consumption. However, the deployment of intermittent renewable sources will inevitably lead to frequent imbalance between supply and demand, as exemplified by the difficulties in maintaining system balance due to wind power variability [4]. Signal processing is certain to play a significant role in dealing with the complexity and uncertainty associated with the smart grid, with stochastic models being a natural choice.

Unexpected frequency variations from the nominal value can trigger abnormal power system conditions that can propagate and aggregate. Accurate and fast frequency tracking is a prerequisite to the system responding quickly to such problems [5], [6]. Approaches to frequency estimation from a single phase result in nonunique solutions, and robust frequency estimators should consider all of the three-phase voltages [7]. For instance, the $\alpha\beta$ transform produces a complex-valued signal from the three-phase voltages [8], where system frequency is obtained from the phase of this signal.

Complex domain solutions for frequency tracking include phase-locked loops (PLLs) [9], least squares [10], demodulation methods [11], and Kalman filtering [12]. Recently, adaptive tracking algorithms based on the minimization of mean square error (MSE) have become a standard, as they are naturally suited to deal with noise, harmonics, and nonstationary environments [10], [13]. However, unbalanced events make it difficult to calculate phase angle [14], [15], as in this case the complex-valued signal obtained from an unbalanced three-phase voltage source is represented as an orthogonal sum of positive (reflecting the energy transfer between generators and consumers) and negative (indicating imbalance between three-phase voltages) sequences. Standard complex linear adaptive filters can only cater for the positive sequences, whereas the negative sequences introduce a modeling error that oscillates at twice the system frequency [16], [17].

This work addresses adaptive tracking of system frequency in the three-phase system and proposes next-generation solutions for fault identification and troubleshooting in the following events that lead to frequency deviations:

- *Imbalance in the generation (G) and load (L).* In the smart grid, the system will frequently switch between the main grid (MG) and microgrids (μG), with parts of the system completely switching off the MG for prolonged periods of time (islanding). The system frequency rises for G > L and decreases for G < L.
- *Single- and dual-phase faults.* The system frequency is derived from the relationship between the three-phase voltages (using Clarke's transform [8]). Faults in one or two phases and voltage sags (sudden drop in voltage for a short period of time) will cause an incorrect frequency estimate and alarm spread through the system, although the actual system frequency was correct.
- *Dual character of load-supply.* The smart grid employs dynamic loads and dual load-generator devices, such as PEVs, which can give the energy back to the grid in the case of emergency. Frequent switching will cause problems with reactive power, whose drifting causes oscillations of power levels and harmonics in frequency.
- *Harmonics.* Some loads (power supplies, motors, heating elements) have nonlinear $V - I$ characteristics and introduce harmonics, which may be slowly floating and not integer multiplies of system frequency. They may cause resonance in the system leading to significant increase in currents and overheating of transformers [18]. Switching on the shunt capacitors for reactive power compensation also causes strong transients and harmonics that are damaging to some equipment.
- *Transient stability issues.* Faults and short circuits could trigger instability, and actions such as shedding loads (or generators) that are needed to mitigate the problem require accurate frequency estimation.

Some of the above events could be dealt with if detected in time, however, current systems do not have sufficient information about the state at the distribution end to do so. This applies particularly to problems related to the management of single- and dual phase faults, short duration voltage sags, and reactive power—these cause harmonics, false alarms congesting the system, and slow response to critical events.

To this end, we introduce a robust framework for adaptive frequency estimation under unbalanced system conditions, a typical case in microgrids, coupled microgrids, and power islands. We first analyze the complex-valued signal, obtained by the $\alpha\beta$ transformation of a three-phase power system, and illustrate the suitability of complex valued filters in this context by illuminating their magnitude-phase relationship and tracking abilities. We then address the geometry of learning to leverage between magnitude-only and phase-only adaptive tracking, and demonstrate the tradeoff between bias and variance of such adaptive frequency estimators. It is further illustrated that under unbalanced system conditions the $\alpha\beta$-transformed complex voltage signal is second-order noncircular (improper), for which current, strictly linear, complex-valued adaptive estimators are suboptimal. A second-order optimal adaptive widely linear frequency estimator is next introduced, and is shown to cater for both the balanced and unbalanced system conditions and to produce unbiased estimates with greatly reduced variance, asymptotically approaching the Cramer-Rao lower bound (CRLB) for high signal to noise ratios. Experimental results include both benchmark and real world case studies, addressing frequency estimation in several typical unbalanced system conditions.

FROM THE HIERARCHICAL GRID TO THE SMART GRID

The operation of the power system at a constant frequency is maintained by regulating the balance between generation and load in real time. Figure 1 shows a simplified diagram of the transmission and distribution part of the grid, illustrating the available loads (L), generators (G), and measurements ($\mathcal{M}$) at both the substation and consumer level. Phasor measurement units (PMUs) provide synchronized measurements of the three-phase voltages, currents, system frequency, and loads; conventional units and PMUs are deployed at the substations and forward synchronized data to the main station. This part is well modeled, however, at
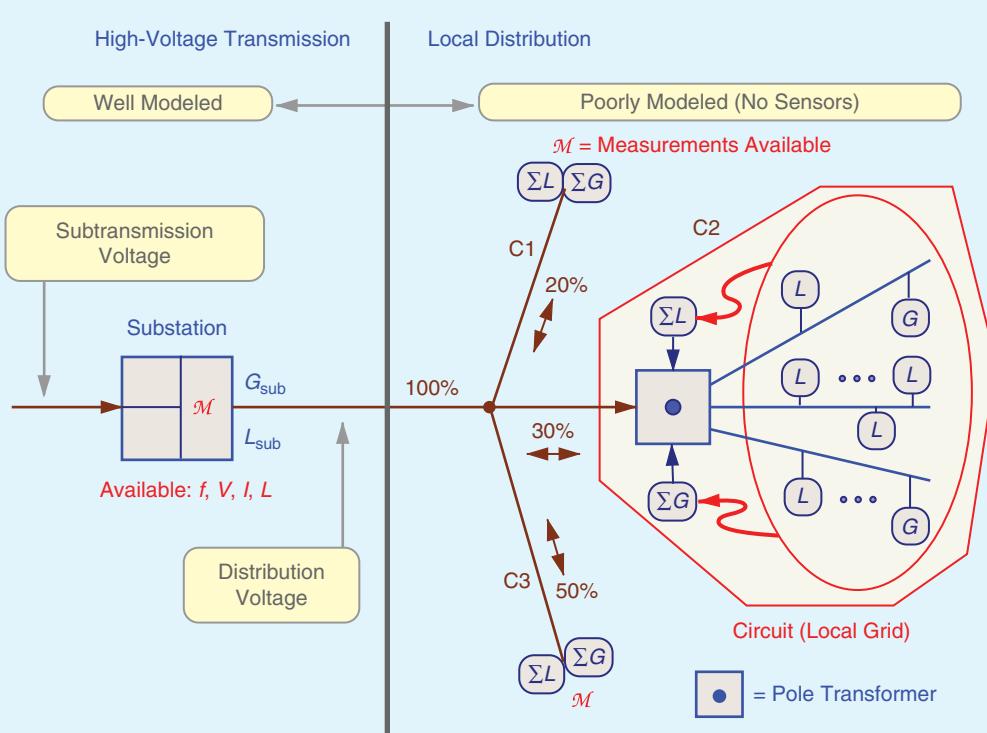
[FIG1] Nodal estimation. Various loads (L) and small generators (G) operate locally and contribute to the variability of power quality. A substation has three to five circuits. The sum of all the circuit loads ΣL and all the generation ΣG equals that of the substation. A G-L mismatch in one circuit is compensated from the generation in another circuit or from the main grid.

present the transmission side of the grid does not have sufficient information about the behavior at the distribution level to incorporate it into the operator model. The progress towards microgrids, coupled microgrids, and islanding will introduce numerous problems related to power quality, whose rectification requires more metering devices at the distribution and consumer level. For instance, photovoltaic sources that produce $1 \sim 2$ kW are often located at the customer's site; they offset the connection load and can also feed the energy back into the grid [19].

MICROGRIDS AND ENERGY ISLANDS

Microgrids are small connected clusters within the main grid, which operate in parallel to the grid or isolated (as an energy island). They respond to fault events autonomously and based on only local information, and facilitate the implementation of key smart grid functions, such as load control, reliability and self-healing, and a greater use of renewables. Microgrids will disconnect when the power quality of the main grid is below certain standards, switching to the islanding mode in the case of faults (dynamic islanding), such as large voltage sags and power outages. It is desirable for the microgrid to seamlessly change its mode of operation between an island and a grid resource; this requires local stability and constant monitoring of large circulating reactive currents between sources, together with voltage versus power droop control. In this way:

■ In normal operation, the loads in microgrid receive power from both the main grid and local generators. When the grid

power is lost, the microgrid dynamically transforms into the islanding mode.
■ If the microgrid was taking the energy from the grid, local generation needs to increase the available power, resulting in a temporary drop in microgrid frequency.
■ If islanding occurred while μG was exporting power to the MG, the microgrid frequency temporarily increases.

VOLTAGE SAGS

Voltage sags refer to a temporary drop in the one- or two-phase voltages for several hundreds of milliseconds [3]. Despite their short duration, they are harmful to a range of equipment, including computers, adjustable speed devices, and three-phase loads. A voltage sag is defined by the IEEE Standard 1159-1995 as a "decrease in root mean square (RMS) voltage at the power frequency for durations from 0.5 cycles to 1 minute." Three-phase sags can be symmetric, for instance, when starting a large motor in an industrial plant, or unbalanced as when energizing a large transformer. Sags that occur at the higher voltage (transmission) side are spread to the lower voltage systems (distribution side) through transformers, also sags and faults that appear at one circuit of the distribution side will affect other circuits at the same substation (see Figure 1). When one line voltage goes into a sag, the other two go into a swell (increase in voltage) to maintain the power required by the load. Since the system frequency is estimated from the three-phase voltages, this poses a major problem.

COMPLEX FORM OF THE THREE-PHASE VOLTAGES

The voltages of a three-phase power system in a noise-free environment can be represented in the discrete time form as

$$v_a(k) = V_a(k)\cos(\omega k \triangle T + \phi)$$

$$v_b(k) = V_b(k)\cos\left(\omega k \triangle T + \phi - \frac{2\pi}{3}\right)$$

$$v_c(k) = V_c(k)\cos\left(\omega k \triangle T + \phi + \frac{2\pi}{3}\right), \quad (1)$$

where $V_a(k), V_b(k), V_c(k)$ are the peak values of each phase voltage component at time instant k, $\triangle T$ is the sampling interval, ϕ is the phase of the fundamental component, $\omega = 2\pi f$ is the angular frequency of the voltage signal, and f is the system frequency. Direct estimation of power quality parameters from the individual phase voltages in (1) is not practical, and it is difficult to select the most representative phase since six different phase voltages exist in a three-phase system when also line-to-line voltages are considered. Solutions operating simultaneously on all the three phases employ invertible transformations, which cast the original system to a physically meaningful transform domain.

To this end, Clarke's transform employs the orthogonal $\alpha\beta0$ transformation matrix [8] to map the time-dependent three-phase voltage into a zero-sequence v_0 and the direct- and quadrature-axis components, v_α and v_β, as

$$\begin{bmatrix} v_0(k) \\ v_\alpha(k) \\ v_\beta(k) \end{bmatrix} = \sqrt{\frac{2}{3}} \begin{bmatrix} \frac{\sqrt{2}}{2} & \frac{\sqrt{2}}{2} & \frac{\sqrt{2}}{2} \\ 1 & -\frac{1}{2} & -\frac{1}{2} \\ 0 & \frac{\sqrt{3}}{2} & -\frac{\sqrt{3}}{2} \end{bmatrix} \begin{bmatrix} v_a(k) \\ v_b(k) \\ v_c(k) \end{bmatrix}. \quad (2)$$

For a balanced system, $V_a(k) = V_b(k) = V_c(k)$ and thus $v_0(k) = 0$, $v_\alpha(k) = A\cos(\omega k \Delta T + \phi)$, and $v_\beta(k) = A\cos(\omega k \Delta T + \phi + \frac{\pi}{2})$, where $A = \text{const}$, and $v_\alpha(k)$ and $v_\beta(k)$ are the orthogonal coordinates of a point whose position is time variant at a rate proportional to the system frequency. In practice, only v_α and v_β are used and the resulting complex voltage signal $v(k)$ is given by [11]

$$v(k) = v_\alpha(k) + \jmath v_\beta(k), \quad (3)$$

where $\jmath = \sqrt{-1}$. There is no loss in information in using this representation, and this voltage also serves as the desired signal in adaptive frequency estimation and can be calculated iteratively from

$$v(k+1) = Ae^{\jmath(\omega(k+1)\Delta T + \phi)} = v(k)e^{\jmath\omega\Delta T}. \quad (4)$$

COMPLEX CIRCULARITY AND WIDELY LINEAR MODELS

We shall now introduce a general framework for both the strictly linear and widely linear complex-valued frequency estimation, based on the complex voltage in (4).

Complex circularity is a property of probability density functions (pdf), indicating that the distributions of a complex random variable x and its rotation $e^{\jmath\varphi}$x are equal for any rotation angle φ. Real-world complex-valued signals are typically noncircular, and for their description we usually consider second-order circularity (properness) and second-order noncircularity (improperness), notions related to the powers in the real and imaginary part (for an overview, see [20]).

WIDELY LINEAR MODELING

Consider a real-valued conditional MSE estimator

$$\hat{y} = E[y|\mathbf{x}], \quad (5)$$

which estimates the signal y in terms of another vector-valued observation $\mathbf{x}$. For zero mean, jointly normal y and $\mathbf{x}$, the optimal solution is the linear estimator given by

$$\hat{y} = \mathbf{x}^T\mathbf{h}, \quad (6)$$

where $\mathbf{h} = [h_1, \ldots, h_L]^T$ is a vector of fixed filter coefficients, $\mathbf{x} = [x_1, \ldots, x_L]^T$ the regressor vector, and $(\cdot)^T$ the vector transpose operator.

In the standard, strictly linear estimation in the complex domain, it is assumed that we can use the same form

$$\hat{y} = \hat{y}_r + \jmath\hat{y}_i = \mathbf{x}^T\mathbf{h}, \quad (7)$$

where the subscripts r and i denote respectively the real and imaginary parts of a complex variable. Since both the real and imaginary parts of complex variables are real, $\hat{y} = E[y_r|\mathbf{x}_r, \mathbf{x}_i] + \jmath E[y_i|\mathbf{x}_r, \mathbf{x}_i]$. Substitute $\mathbf{x}_r = (\mathbf{x} + \mathbf{x}^*)/2$ and $\mathbf{x}_i = (\mathbf{x} - \mathbf{x}^*)/2\jmath$ to arrive at

$$\hat{y} = E[y_r|\mathbf{x}, \mathbf{x}^*] + \jmath E[y_i|\mathbf{x}, \mathbf{x}^*] = E[y|\mathbf{x}, \mathbf{x}^*] \quad (8)$$

giving the widely linear estimator for complex valued data

$$\hat{y} = \mathbf{h}^T\mathbf{x} + \mathbf{g}^T\mathbf{x}^* = \mathbf{x}^T\mathbf{h} + \mathbf{x}^H\mathbf{g} = \mathbf{x}^T\mathbf{w}^a, \quad (9)$$

where $\mathbf{h}$ and $\mathbf{g}$ are complex-valued coefficient vectors. In practice, this estimator uses a regressor vector produced by concatenating the input vector $\mathbf{x}$ with its conjugate $\mathbf{x}^*$, to give an augmented input vector $\mathbf{x}^a = [\mathbf{x}^T, \mathbf{x}^H]^T$, and similarly the augmented coefficient vector $\mathbf{w}^a = [\mathbf{h}^T, \mathbf{g}^T]^T$.

AUGMENTED COMPLEX STATISTICS

The $2L \times 2L$ augmented covariance matrix, corresponding to the widely linear model in (9), now becomes [20]–[22]

$$\mathbf{C}_{\mathbf{xx}}^a = E\begin{bmatrix} \mathbf{x} \\ \mathbf{x}^* \end{bmatrix} [\mathbf{x}^H \mathbf{x}^T] = \begin{bmatrix} \mathbf{C}_{\mathbf{xx}} & \mathbf{P}_{\mathbf{xx}} \\ \mathbf{P}_{\mathbf{xx}}^* & \mathbf{C}_{\mathbf{xx}}^* \end{bmatrix} \quad (10)$$

and contains the full second-order statistical information. Observe that the covariance matrix, $\mathbf{C}_{\mathbf{xx}} = E[\mathbf{xx}^H]$, alone does not have sufficient degrees of freedom to explain complete second-order information, and to capture the second-order information we also need to consider the pseudocovariance matrix, $\mathbf{P}_{\mathbf{xx}} = E[\mathbf{xx}^T]$. Processes
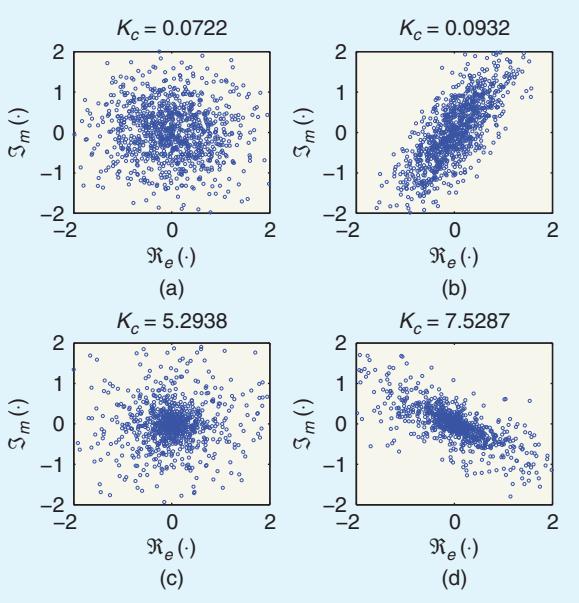
[FIG2] Circularity plots for complex doubly white noises. (a) circular Gaussian, (b) noncircular Gaussian ($\eta = 0.81$), (c) circular Laplacian noise, and (d) noncircular Laplacian ($\eta = 0.81$). Symbol K_c denotes the kurtosis.

with the vanishing pseudocovariance, $\mathbf{P_{xx}} = \mathbf{0}$, are termed second-order circular (or proper). Therefore, the widely linear estimator in (9) is optimal for the generality of complex signals (both proper and improper), and simplifies into the strictly linear model in (7), for which $\mathbf{g} = \mathbf{0}$, for proper data.

INDEX OF IMPROPERNESS
The degree of improperness can be calculated using the circularity index, given by [23]
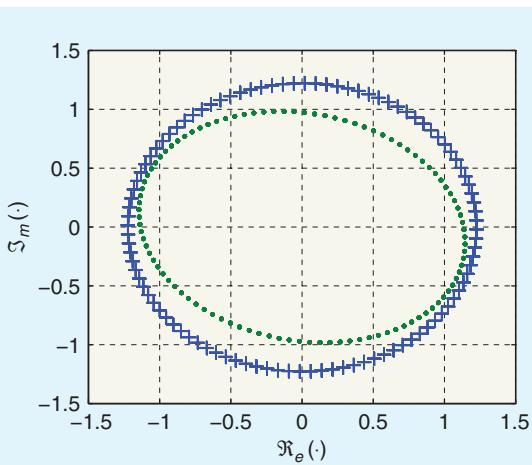
[FIG3] Circularity via the "real-imaginary" ($\Re - \Im$) scatter plot. The blue circle denoted by "+" corresponds to a circular $v(k)$ in a balanced system ($V_a(k) = V_b(k) = V_c(k)$) at 1 per unit (p.u.). The green ellipse denoted by " · " corresponds to a noncircular $v(k)$ stemming from an unbalanced system with $V_a(k) = 1$ p.u., $V_b(k) = 0.9$ p.u., and $V_b(k) = 0.7$ p.u.

$$\eta = \frac{|\tau_x|^2}{\sigma_x^2}, \qquad (11)$$

where $\sigma_x^2 = E[x(k)x^*(k)]$ is the variance of the signal x and $\tau_x^2 = E[x(k)x^T(k)]$ the pseudovariance of x. Note that $\eta \in [0, 1]$, with $\eta = 0$ a second-order circular (proper) $x(k)$, and a second-order noncircular (improper) $x(k)$ for $\eta > 0$. Examples of circular and noncircular doubly white noises, together with their kurtosis values K_c, are given in Figure 2, where the symbol $\Re(\cdot)$ denotes the real and $\Im(\cdot)$ the imaginary part of a complex number. For the assessment of noncircularity in real time, we refer to [24].

WIDELY LINEAR AUTOREGRESSIVE MODELING
Based on (9), the widely linear autoregressive (WLAR) model is given by

$$y(k) = \mathbf{h^T}(k)\mathbf{x}(k) + \mathbf{g^T}(k)\mathbf{x}^*(k) + n(k), \quad n \sim \mathcal{N}(0, \tau_x^2, \sigma_x^2).$$

Its coefficients are obtained from the widely linear Yule-Walker equations, given by [24]

$$\begin{bmatrix} \mathbf{h}^* \\ \mathbf{g}^* \end{bmatrix} = \begin{bmatrix} \mathbf{C} & \mathbf{P} \\ \mathbf{P}^* & \mathbf{C}^* \end{bmatrix}^{-1} \begin{bmatrix} \mathbf{c} \\ \mathbf{p}^* \end{bmatrix}. \qquad (12)$$

The advantage of widely linear over strictly linear estimation can be quantified by the difference between their corresponding MSEs, e_L^2 and e_{WL}^2, given by

$$\delta e^2 = e_L^2 - e_{WL}^2 \geq 0, \qquad (13)$$

which is strictly positive for improper data and zero for proper data [20], [22]. Thus, widely linear estimators have a performance advantage over their strictly linear counterparts for improper data: their performances for proper data are identical [20].

VOLTAGE SAGS AND NONCIRCULARITY
It is now possible to relate complex circularity with the distribution of the $\alpha\beta$ voltage $v(k)$ in (3), both in balanced and unbalanced system conditions. Figure 3 shows the amplitude distribution diagrams for a balanced case and an unbalanced voltage sag event. When the phase voltages exhibit dips or transients (a sag event), $V_a(k)$, $V_b(k)$, $V_c(k)$ are not identical and samples of $v(k)$ are located on an ellipse (noncircular), whereas for a balanced system the distribution of $v(k)$ remains on a circle (circular).

From Figure 3, observe that by accounting for second-order (non)circularity, it is possible in principle to identify the type and parameters of a voltage sag within a quarter of frequency cycle, providing a very fast indication of a system fault [25].

FREQUENCY ESTIMATION MODELS IN BALANCED AND UNBALANCED THREE-PHASE SYSTEMS
The current state of the art is based on the $\alpha\beta$ voltage in (3) and the subsequent application of the stochastic gradient-based complex least mean square (CLMS) algorithm. Such

algorithms aim to minimize the instantaneous error power $\mathcal{J}(k) = e(k)e^*(k) = |e(k)|^2$, using a gradient descent-based update of the filter coefficient vector $\mathbf{w}(k)$, in the form

$$\mathbf{w}(k+1) = \mathbf{w}(k) - \mu \nabla_{\mathbf{w}} \mathcal{J}(k) \overset{\text{CLM}}{=} \mathbf{w}(k) + \mu e(k)\mathbf{x}^*(k), \quad (14)$$

where μ is a small positive learning rate, $e(k)$ the output error of the filter, $y(k) = \mathbf{x}^T(k)\mathbf{w}(k)$ the filter output, and $\mathbf{x}(k)$ the filter input vector (regressor vector).

THE STRICTLY LINEAR CLMS MODEL

For adaptive frequency estimation based on the $\alpha\beta$ voltage in (3), we only need a single filter coefficient [10], thus all the estimators will have this form. Upon solving (14), the CLMS-based model becomes

$$\hat{v}(k+1) = w(k)v(k)$$
$$e(k) = v(k+1) - \hat{v}(k+1)$$
$$w(k+1) = w(k) + \mu e(k)v^*(k), \quad (15)$$

where the filter weight $w(k)$ estimates the phasor $e^{j\omega\Delta T}$ in (4), $\hat{v}(k+1)$ is the estimate of $v(k+1)$, and the estimated instantaneous system frequency is derived from

$$\hat{f}(k) = \frac{1}{2\pi\Delta T} \sin^{-1}(\Im(w(k))) \quad (16)$$

based on the evolution of the coefficient $w(k)$ of the strictly linear adaptive estimator in (15).

This algorithm aims to minimize both the amplitude and phase error, however, it is often advantageous to perform estimation based on phase-only or magnitude-only information.

GEOMETRY OF LEARNING IN THE COMPLEX DOMAIN

From (16), the instantaneous system frequency estimate is obtained from the phase in $e^{j\omega\Delta T}$, that is, in balanced conditions it is primarily the phase rather than the magnitude that conveys useful information. However, in unbalanced conditions the magnitude should also be taken into account.

The least mean magnitude phase (LMMP) algorithm [26] decomposes the cost function in $\mathcal{J} = e(k)e^*(k)$ into the magnitude-only, $\mathcal{J}_m$, and phase-only, $\mathcal{J}_p$, parts as

$$\mathcal{J}(d,y) = \mu_1 \mathcal{J}_m(d,y) + \mu_2 \mathcal{J}_p(d,y) = |e(k)|^2, \quad (17)$$

where for the standard CLMS $\mu_1 = \mu_2 = \mu$, the teaching signal $d(k) = y(k) + e(k)$, and the costs ($\angle$ is the angle operator)

$$\mathcal{J}_m(d,y) = (|d| - |y|)^2$$
$$\mathcal{J}_p(d,y)|\angle d - \angle y|^2 = 2|d||y|(1-\cos(\angle d - \angle y)). \quad (18)$$

By weighting the terms in (18), the LMMP (shaded area in Figure 4) leverages between magnitude-only and phase-only estimation, and spans a whole range of algorithms, including the standard CLMS, denoted by y_{clms}, and the least mean phase (LMP) algorithm, y_{lmp} [27], [13]. Figure 4 illuminates the

geometry of learning: the phase only estimate, y_{lmp}, corrects for the phase but cannot deal with magnitude changes, whereas the magnitude only estimate, y_{cma}, corrects only for the magnitude and not for the phase changes.

The update of the complex LMP algorithm is given by

$$w_{\text{lmp}}(k+1) = w_{\text{lmp}}(k) + \frac{\jmath\mu e_{\text{pe}}(k)v^*(k)}{\left(v(k)w_{\text{lmp}}(k)\right)^*} \quad (19)$$

while the complex LMMP update is

$$w_{\text{lmmp}}(k+1) = w_{\text{lmmp}}(k) + \mu_m(|v(k+1)|\text{sgn}(\hat{v}(k+1))$$
$$- \hat{v}(k+1))v^*(k) + \mu_p(v(k+1)$$
$$- |v(k+1)|\text{sgn}(\hat{v}(k+1)))v^*(k), \quad (20)$$

where μ_m and μ_p are the respective stepsizes and $\text{sgn}(\cdot)$ is the sign operator.

THE ACLMS-BASED FREQUENCY ESTIMATION

Figure 3 shows that in unbalanced conditions the voltage in (3) is noncircular and is adequately modeled only by using the widely linear model in (9), whose adaptive version is (see [25] and "Noncircularity Under Unbalanced Conditions")

$$v(k) = A(k)e^{\jmath(\omega k\Delta T + \phi)} + B(k)e^{-\jmath(\omega k\Delta T + \phi)}. \quad (21)$$

In other words, when the phase voltages $V_a(k)$, $V_b(k)$, $V_c(k)$ are not identical, $A(k)$ is no longer a constant, $B(k) \neq 0$, and the standard strictly linear model in (4) is not adequate. The coefficients of the widely linear estimator can be adapted using the augmented CLMS (ACLMS), given by [20] and [28]

$$\text{Estimator: } \hat{v}(k+1) = \underbrace{v(k)h(k)}_{\text{standard part}} + \underbrace{v^*(k)g(k)}_{\text{conjugate part}}$$
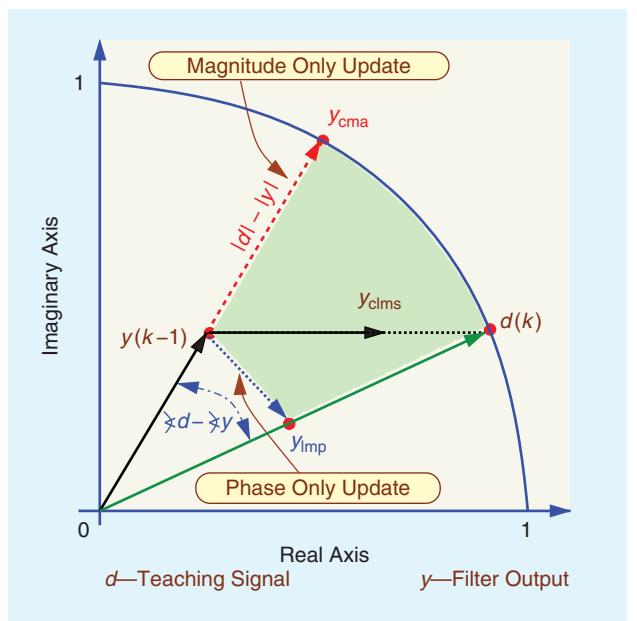
NONCIRCULARITY UNDER UNBALANCED CONDITIONS
For the three-phase system in (1) and (2), the complex-valued $v(k) = v_\alpha(k) + Jv_\beta(k)$ comprises the standard part (left-hand term) and the conjugate part (right-hand term), that is

$$v(k) = A(k)e^{J(\omega k \Delta T + \phi)} + B(k)e^{-J(\omega k \Delta T + \phi)}, \quad \text{(S1)}$$

where

$$A(k) = \frac{\sqrt{6}(V_a(k) + V_b(k) + V_c(k))}{6}$$

$$B(k) = \frac{\sqrt{6}(2V_a(k) - V_b(k) - V_c(k))}{12}$$

$$- \frac{\sqrt{2}(V_b(k) - V_c(k))}{4} J.$$

Figure 3 shows that $v(k)$ is second-order circular with a rotation invariant probability density function in the complex plane if $B(k) = 0$ and $A(k)$ is a constant. This can be achieved only when $V_a(k), V_b(k), V_c(k)$ are identical at each time instant, when (S1) simplifies into (4). In unbalanced conditions, $A(k)$ is real valued, but $B(k) \neq 0$ and can be complex valued, resulting in a second-order noncircular (improper) $v(k)$.

Update: $h(k + 1) = h(k) + \mu e(k)v^*(k)$

$$g(k + 1) = g(k) + \mu e(k)v(k). \quad \text{(22)}$$

The stability of ACLMS has been investigated in [29]. From (21) and (22), the estimate $\hat{v}(k + 1)$ becomes

$$\hat{v}(k + 1) = (A(k)h(k) + B^*(k)g(k))e^{J(\omega k \Delta T + \phi)}$$
$$+ (A^*(k)g(k) + B(k)h(k))e^{-J(\omega k \Delta T + \phi)}. \quad \text{(23)}$$

Comparing the corresponding terms in (21) and (23), we have

$$e^{J\hat{\omega} \Delta T} = \frac{A(k)g^*(k) + B^*(k)h^*(k)}{B^*(k+1)}. \quad \text{(24)}$$

Using the assumption held implicitly in frequency estimation that at two consecutive time instants, $A(k + 1) \approx A(k)$, and also $B(k + 1) \approx B(k)$, after some algebraic manipulation (for more detail and MATLAB sources, see [30]), we arrive at the widely linear three phase system frequency estimate

$$\hat{f}(k) = \frac{1}{2\pi\Delta T} \sin^{-1}(\Im(h(k) + a_1(k)g(k))). \quad \text{(25)}$$

This is a widely linear extension of the standard, strictly linear, estimator in (16). When the system is balanced, $v(k)$ is circular, $g(k) = 0$, and we have the standard solution in (16).

UNBALANCED SYSTEM CONDITIONS: VOLTAGE SAGS
There are seven typical three-phase voltage sags that cause system imbalance: four single-phase-to-ground sags and three two-phase-to-ground sags. The phasor diagrams for the former case,

Type A   Type B

Type C   Type D

Phasor Diagrams
(a)

Type A   Type B

Type C   Type D

Circularity Plots
(b)
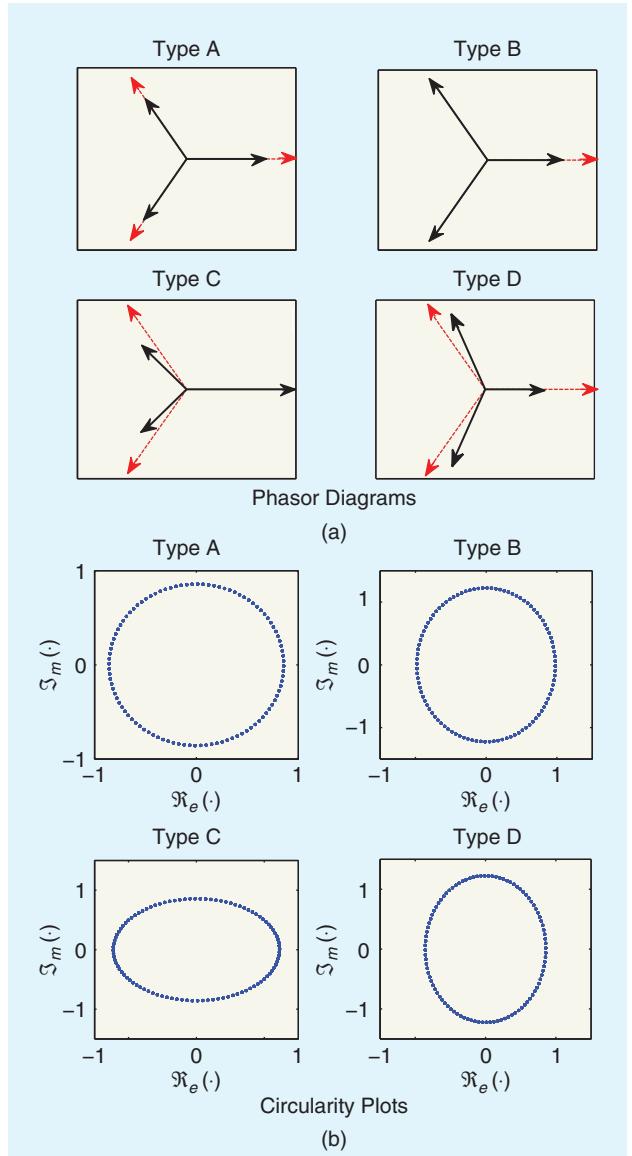
[FIG5] Unbalanced voltage sags due to single phase-to-ground faults, for the characteristic voltage of $V = 0.7$. (a) Phasor diagram (dotted line denotes balanced operation) and (b) circularity via a "real-imaginary" plot.

together with the associated circularity plots, are shown in Figure 5. Observe that apart from the symmetric Type A voltage sag, all the other sags exhibit noncircular amplitude distributions and the frequency drifts are thus expected to be best modeled by widely linear models. The shape, orientation, and principal axes of circularity diagrams reveal the type of sags, allowing us more degrees of freedom compared to standard frequency estimation and enabling us to identify a fault based on its circularity properties in as little as 1/4 of the cycle. For instance, Type C sag is noncircular and aligned horizontally, whereas Type B sag is noncircular and aligned vertically. Similar observations can be made for the two-phase-to-ground faults; for more details, see [30].

WIDELY LINEAR FREQUENCY ESTIMATION

The following situations occur frequently in practical frequency estimation and will be addressed in this section.

■ frequency estimation in the presence of voltage sags, where the system frequency remains at 50 Hz, but due to system imbalance the frequency estimate is wrong

■ frequency rise and decay, due to a mismatch between production and consumption (microgids, islands)

■ harmonics caused by certain loads and imbalance of active and reactive power (renewables, microgrids).

Simulations were performed for signals sampled at 5 kHz, and the step-size was $\mu = 0.01$ in all simulations.

BALANCED SYSTEM OPERATION

In the first set of simulations, the power system was balanced and was operating at the system frequency $f = 50$ Hz, and all the considered algorithms were initialized with $f_0 = 50.5$ Hz. Table 1 shows that the strictly linear CLMS and LMP and the widely linear ACLMS had similar performances in terms of the error percentage over a range of SNR. The phase-only LMP outperformed CLMS, as it was designed to deal effectively with the phase information and the frequency is estimated from the phase in (16).

FREQUENCY ESTIMATION: VOLTAGE SAGS

Figure 6 compares performances of the strictly linear CLMS, LMP, and LMMP for a system with Type C voltage sag (with characteristic complex voltage $V = 0.7$) occurring at $t = 0.05$ s, having a 12% voltage drop and 9.5° phase angle offset for phases v_b and v_c. This led to an unbalanced system with a degree of noncircularity $\eta = 0.3501$ (see Figure 5). The LMMP algorithm showed smallest variation whereas the phase error-based LMP algorithm was the only unbiased algorithm. None was optimal for the noncircular unbalanced three-phase system.

FREQUENCY ESTIMATION: HARMONICS AND CASCADED EVENTS

Figure 7 illustrates the behavior of ACLMS, LMP, and CLMS for a system undergoing a sequence of harmful events. At $t = 0.05$ s, a Type C sag occurred, with around a 12% voltage drop and 9.5° phase angle offset in phases v_b and v_c, leading to an unbalanced system with a degree of circularity $\eta = 0.3501$ (see Figure 5). There was an inevitable oscillation error at twice of the system frequency for both the CLMS- and LMP-based estimation due to the undermodeling (see "Suboptimality of Strictly Linear Estimators"). The phase error-based LMP algorithm did not exhibit the bias encountered by CLMS, whereas the advantage of the widely linear ACLMS-based estimator in accurately estimating the frequency can be seen after convergence (after about 100 ms). Then at $t = 0.25$ s, a Type D sag took place exhibiting a 30% voltage drop for phase v_a and 6.6% voltage drop for both the phases v_b and v_c, together with a 8° phase angle offset, exhibiting the degree of noncircularity of $\eta = 0.3433$. Again, the widely linear ACLMS gave an unbiased estimate, whereas the CLMS was not adequate. Finally, after $t = 0.4$ s, a 10% of the third harmonic and 10% of the fifth harmonic of the fundamental frequency

[TABLE 1] ABSOLUTE ERROR % FOR THE ESTIMATION IN BALANCED SYSTEMS.

SNR [DB]	50	40	30	20	10
CLMS	0.047%	0.17%	0.53%	2.73%	14.73%
LMP	0.032%	0.11%	0.33%	1.05%	13.72%
ACLMS	0.048%	0.17%	0.53%	1.83%	13.21%
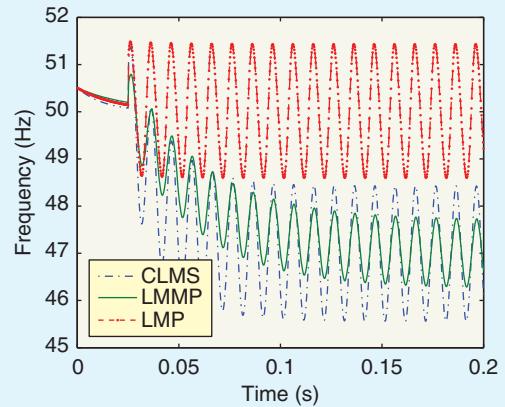
[FIG6] Frequency estimation for Type C voltage sag.

were added into the unbalanced system suffering from the same Type D sag to give the circularity index of $\eta = 0.3920$. The ACLMS achieved significantly better performance with a smaller oscillation error than the strictly linear CLMS and LMP.

FREQUENCY ESTIMATION: SUPPLY-DEMAND MISMATCH

Figure 8 illustrates the superior performance of the widely linear ACLMS over CLMS for a power system experiencing frequency rise and decay due to the G-L mismatch. In the simulations, the 50 Hz frequency estimate was offset by a Type D unbalanced three-phase voltage sag, and the frequency rose and decayed at a rate of 5 Hz/s. The ACLMS algorithm followed the true system frequency very closely after an initialization period of around 0.05 s, whereas CLMS produced a biased estimate with large error variance.
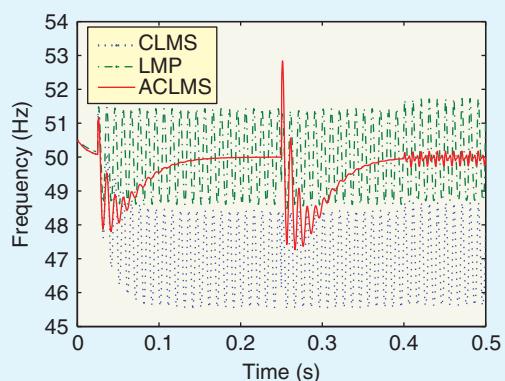
[FIG7] Frequency estimation for a cascade of harmful events: strictly linear CLMS and LMP versus widely linear ACLMS.

SUBOPTIMALITY OF STRICTLY LINEAR ESTIMATORS

Here we give theoretical justification for the suboptimality of standard, strictly linear, complex adaptive filters for frequency estimation in unbalanced three-phase voltage systems. In any unbalanced condition, the expression (21) stands, and the estimator $\hat{v}(k+1)$ obtained using strictly adaptive algorithms, such as CLMS, LMMP, and LMP can be expressed as

$$\hat{v}(k+1) = (A(k)e^{J(\omega k \Delta T + \phi)} + B(k)e^{-J(\omega k \Delta T + \phi)})w(k).$$

In the steady state, $\hat{v}(k+1) \approx v(k+1)$, resulting in

$$w(k) = \frac{A(k+1)e^{J(\omega k \Delta T + \phi)}e^{j\omega \Delta T}}{A(k)e^{J(\omega k \Delta T + \phi)} + B(k)e^{-J(\omega k \Delta T + \phi)}}$$

$$+ \frac{B(k+1)e^{-J(\omega k \Delta T + \phi)}e^{-j\omega \Delta T}}{A(k)e^{J(\omega k \Delta T + \phi)} + B(k)e^{-J(\omega k \Delta T + \phi)}}. \quad (S2)$$

Under the standard assumptions that $A(k+1) \approx A(k)$, and $B(k+1) \approx B(k)$, we have (since sampling frequency $\gg$ f)

$$w(k) = e^{-j\omega \Delta T} + \frac{e^{j\omega \Delta T} - e^{-j\omega \Delta T}}{1 + \frac{B(k)}{A(k)}e^{-2J(\omega k \Delta T + \phi)}}, \quad (S3)$$

where $B(k)/A(k)$ is an unknown parameter and $w(k) = w(k + (1/2f\Delta T))$ is periodic. In (16), the function $\sin^{-1}$ is monotonic, resulting in periodic oscillations of the estimated frequency $\hat{f}(k)$. The cycle frequency due to undermodeling is $2f$ when using standard, strictly linear, adaptive filters in unbalanced power systems, whereas for balanced power systems $B(k) = 0$, and the standard linear estimate in (16) is adequate.
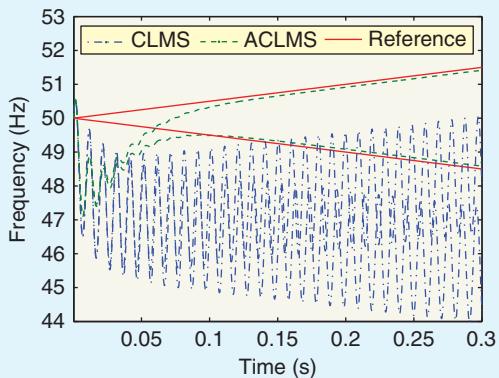
[FIG8] Estimation for a mismatch between generation and consumption (frequency rise and decay). The widely linear ACLMS approached the correct value to within 5% in 50 ms.

THEORETICAL PERFORMANCE BOUNDS

Bias in frequency estimation is particularly damaging, as it indicates nonexisting shifts in frequency (causing alarms), while high estimator variance indicates that the algorithm used was not adequate. Figure 9 shows statistical bias and variance
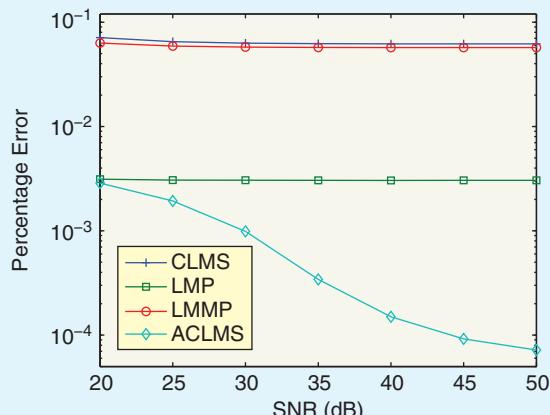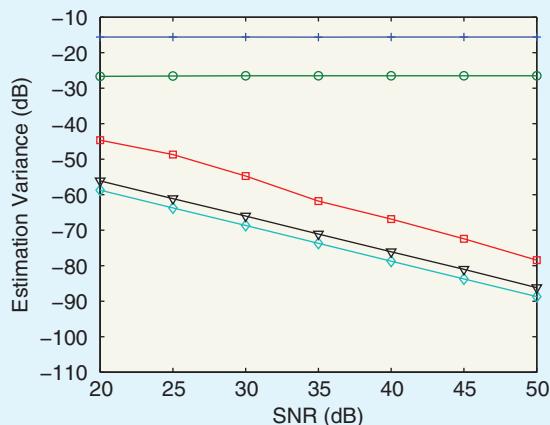
[FIG9] Bias and variance of the widely linear ACLMS, and the strictly linear CLMS, LMP, and LMMP compared to CRLB (curves averaged over 1,000 independent trials). (a) Bias: the widely linear ACLMS is asymptotically unbiased, followed by LMP and (b) variance: the widely linear ACLMS is a consistent estimator.

analysis for all the algorithms considered, conducted in a noisy environment by averaging 1,000 independent trials. The CRLB was calculated for both the frequency as the only unknown parameter (approximate CRLB can be found in [25]) and for a general case (frequency, voltages); for more detail, see [30]. Compared with CLMS and LMMP, the phase error-based LMP achieved smaller bias; the strictly linear CLMS, LMP, and LMMP were inadequate for unbalanced system conditions (noncircular), their bias was not affected by the noise level. The widely linear ACLMS-based estimator was asymptotically unbiased for high SNR. Similar conclusions can be drawn for the estimation variance—the widely linear ACLMS was consistent, approaching the CRLBs to within 9 dB in the high SNR region [see Figure 9(b)].

FREQUENCY ESTIMATION: REAL WORLD VOLTAGE SAGS

Real-world three phase voltage sags were recorded at a 110/20/10 kV transformer station, using the ABB REL 531 numerical line distance protection terminal monitoring "phase-to-ground" voltages. The device was set to record whenever the phase voltage value dropped below 90% of its nominal value for longer than 20 ms, and was sampling at 1 kHz; the voltage waveforms, normalized with respect to their nominal peak values, are shown in Figure 10(a) and (c). In the first case study, a problem in phase v_c occurred (short circuit with earth), causing a 94% voltage drop, while the voltages in phases v_a and v_b kept their nominal values to give a degree of noncircularity of $\eta = 0.8081$ (see Figure 11). In the second case study, at around $t = 0.07$ s, phase v_b experienced a shortcut with earth, resulting in a 65.32% voltage sag and 79.25% and 21.92% voltage swells in phases v_a and v_c respectively, to give a degree of noncircularity of $\eta = 0.2151$ (see Figure 11). Figure 10 shows that CLMS was not adequate for the unbalanced situation, while ACLMS recovered quickly and was able to accurately estimate the true system frequency at 50 Hz, not indicating false alarms.

SUMMARY AND FUTURE OPPORTUNITIES

We have shown that widely linear estimators of instantaneous system frequency are second-order optimal for both balanced and unbalanced three-phase systems. Unlike the strictly linear CLMS, LMP, and LMMP, the widely linear ACLMS has been shown to yield unbiased minimum variance solutions, whereby the performance gain over standard methods increases with the degree of system imbalance (noncircularity of the phasor). This perfectly suits smart grid applications, where severe frequency variations are expected due to the on-off switching of subgrids, dual roles of generators and loads (e.g., PEVs), and false alarms due to voltage sags. Widely linear estimation in this context provides new opportunities, whereby a rigorous account of improperness (second-order noncircularity) of the complex $\alpha\beta$ voltage makes it possible to implement fast, accurate, robust, and statistically enhanced solutions for the following:

■ *Rapid frequency trackers* at the distribution level, which are envisaged to become part of many future appliances—smart loads must be able to detect rapid frequency changes and take appropriate action.

■ *Identification and classification* of system faults from voltage dips, based on their different degrees of noncircularity and shapes of circularity diagrams (see Figures 5 and 11). It is critical that the frequency estimator remains accurate during the fault, in order not to send false alarms, and to indicate whether the system experienced a one-, two-, or three-phase fault.

■ *Rate of change* frequency trackers, which are crucial for the operation of microgrids and in events of islanding.

■ *Loss-of-mains detection* in real time, as a drop in frequency may indicate loss of a generator, and a rise in frequency loss of a load. The way renewables react to these situations depends on the type of voltage sag—the widely linear methodology enables their identification and tracking at the subcycle scale (less than 20 ms).
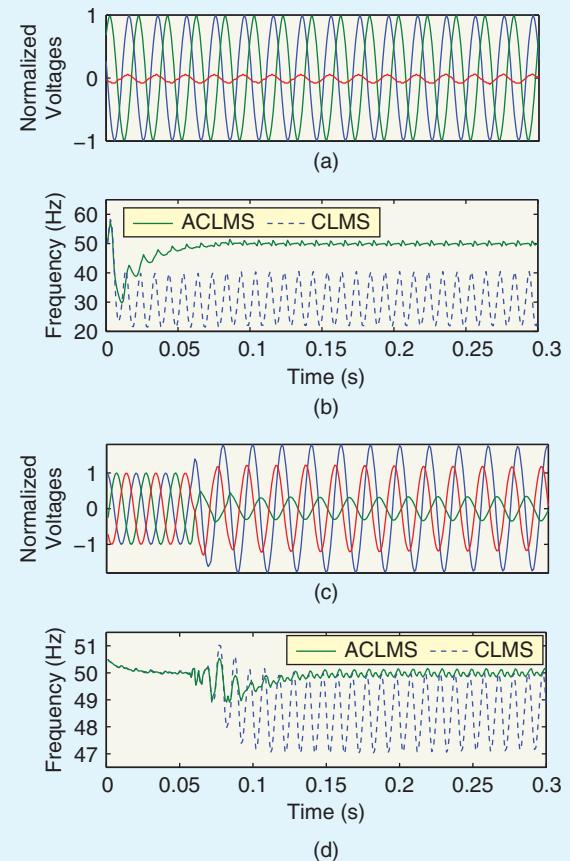
[FIG10] Frequency estimation for real-world voltage sags. (a) Phase C undergoes a voltage dip of 94%, (b) frequency estimation using CLMS (broken) and ACLMS (solid), (c) Phase B experiences a short circuit and Phase A and Phase C go into a swell, and (d) frequency estimation using CLMS (broken) and ACLMS (solid).
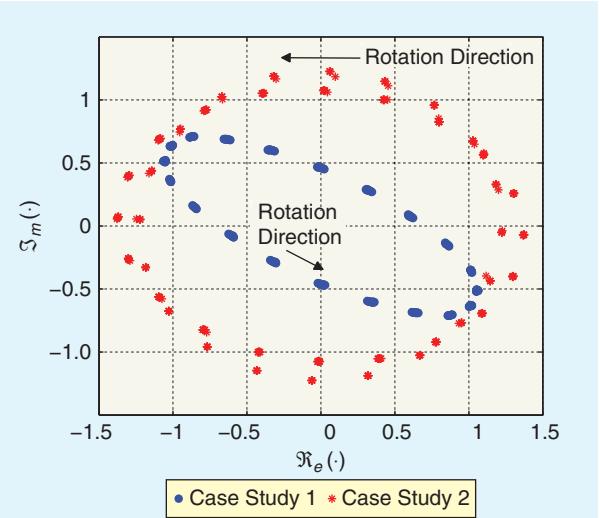
[FIG11] Noncircularity of real world unbalanced voltage sags.

- *Optimal operation of microgrids*: in a cooperative distributed mode, we not only must bring in new generators and dynamically interconnect the grid, but we also remove low priority loads when power quality deteriorates.
- *Low-voltage ride through* and transient stability routines to cater for the bidirectional flow of active and reactive power when renewables are profusely used.
- *More degrees of freedom in scheduling routines*, since small scale renewables are a must-take resource, but are intrinsically intermittent—causing system imbalance.

ACKNOWLEDGMENTS

AUTHORS

Yili Xia (yili.xia06@imperial.ac.uk) received his B.Eng. degree in information engineering from Southeast University, Nanjing, China, in 2006, and the M.Sc. (with distinction) degree in communications and signal processing from the Department of Electrical and Electronic Engineering, Imperial College London, United Kingdom, in 2007. He obtained his Ph.D. degree in widely linear adaptive filtering from Imperial College in 2011, where he is currently working as a research associate. His research interests include complex-valued linear and nonlinear adaptive filters and their applications to power systems.

Scott C. Douglas (douglas@engr.smu.edu) is a professor in the electrical engineering department at Southern Methodist University, Dallas, Texas. He received his B.Sc., M.Sc., and Ph.D. degrees from Stanford University, California, and he has been working in the areas of adaptive filters and blind source separation. He was a recipient of the NSF Career Award and has served on the editorial boards of *IEEE Transactions on Signal Processing, IEEE Signal Processing Letters*, and *Journal of Signal Processing Systems*. He served as a technical chair in several signal processing conferences and as a general chair of ICASSP 2010.

Danilo P. Mandic (d.mandic@imperial.ac.uk) is a professor of signal processing at Imperial College London, United Kingdom. He has been working in the area of nonlinear and multivariate adaptive signal processing and nonlinear dynamics. He has published two research monographs titled *Recurrent Neural Networks for Prediction* and *Complex Valued Nonlinear Adaptive Filters*. He has been a guest professor at KU Leuven, Belgium, a frontier researcher at RIKEN Japan, a member of the IEEE Technical Committee on Signal Processing Theory and Methods, and an associate editor of *IEEE Transactions on Signal Processing* and *IEEE Transactions on Neural Networks*.

REFERENCES

[1] M. De Nigris, I. Gianinoniand, S. Grillo, S. Massucco, and F. Silvestro, "Impact evaluation of plug-in electric vehicles (PEV) on electric distribution networks," in *Proc. 14th Int. Conf. Harmonics and Quality in Power (ICHQP)*, 2010, pp. 1–6.

[2] A. Ipakchi and F. Albuyeh, "Grid of the future," *IEEE Power Energy Mag.*, vol. 7, no. 2, pp. 52–62, 2009.

[3] M. H. J. Bollen, "Voltage sags in three-phase systems," *IEEE Power Eng. Rev.*, vol. 21, no. 9, pp. 8–15, 2001.

[4] J. C. Smith, R. Thresher, R. Zavadil, E. DeMeo, R. Piwko, B. Ernst, and T. Ackermann, "A mighty wind," *IEEE Power Energy Mag.*, vol. 7, no. 2, pp. 41–51, 2009.

[5] O. Vainio and S. Ovaska, "Digital filtering for robust 50/60 Hz zero-crossing detectors," *IEEE Trans. Instrum. Meas.*, vol. 45, no. 2, pp. 426–430, 2001.

[6] L. G. B. Barbosa Rolim, Jr., D. R. Rodrigues da Costa, and M. Aredes, "Analysis and software implementation of a robust synchronizing PLL circuit based on the PQ theory," *IEEE Trans. Ind. Electron.*, vol. 53, no. 6, pp. 1919–1926, 2006.

[7] V. Eckhardt, P. Hippe, and G. Hosemann, "Dynamic measuring of frequency and frequency oscillations in multiphase power systems," *IEEE Trans. Power Delivery*, vol. 4, no. 1, pp. 95–102, 1989.

[8] E. Clarke, *Circuit Analysis of A.C. Power Systems*. New York: Wiley, 1943.

[9] P. Rodriguez, J. Pou, J. Bergas, J. I. Candela, R. P. Burgos, and D. Boroyevich, "Decoupled double synchronous reference frame PLL for power converter control," *IEEE Trans. Power Electron.*, vol. 22, no. 2, pp. 584–592, 2007.

[10] A. K. Pradhan, A. Routray, and A. Basak, "Power system frequency estimation using least mean square technique," *IEEE Trans. Power Delivery*, vol. 20, no. 3, pp. 761–766, 2005.

[11] M. Akke, "Frequency estimation by demodulation of two complex signals," *IEEE Trans. Power Delivery*, vol. 12, no. 1, pp. 157–163, 1997.

[12] P. K. Dash, A. K. Pradhan, and G. Panda, "Frequency estimation of distorted power system signals using extended complex Kalman filter," *IEEE Trans. Power Delivery*, vol. 14, no. 3, pp. 761–766, 1999.

[13] T. K. Rawat and H. Parthasarathy, "A continuous-time least mean-phase adaptive filter for power frequency estimation," *Electr. Power Energy Syst.*, vol. 31, no. 2, pp. 111–115, 2009.

[14] D. Beeman, *Industrial Power System Handbook*. New York: McGraw-Hill, 1955.

[15] L. Zhang and M. H. J. Bollen, "Characterisation of voltage dips in power systems," *IEEE Trans. Power Delivery*, vol. 15, no. 2, pp. 827–832, 2000.

[16] H. S. Song and K. Nam, "Instantaneous phase-angle estimation algorithm under unbalanced voltage-sag conditions," *IEE Proc. Gener., Transm. Distrib.*, vol. 147, no. 6, pp. 409–415, 2000.

[17] M. Mojiri, D. Yazdani, and A. Bakhshai, "Robust adaptive frequency estimation of three-phase power system," *IEEE Trans. Instrum. Meas.*, vol. 59, no. 7, pp. 1793–1802, 2010.

[18] M. H. J. Bollen, I. Y. H. Gu, S. Santoso, M. F. McGranaghan, P. A. Crossley, M. V. Ribeiro, and P. F. Ribeiro, "Bridging the gap between signal and power," *IEEE Signal Processing Mag.*, vol. 26, no. 4, pp. 11–31, 2009.

[19] J. Bebic, R. Wawlling, K. O'Brien, and B. Kroposki, "The sun also rises," *IEEE Power Energy Mag.*, vol. 7, no. 3, pp. 34–44, 2009.

[20] D. P. Mandic and S. L. Goh, *Complex Valued Nonlinear Adaptive Filters: Noncircularity, Widely Linear and Neural Models*. Hoboken, NJ: Wiley, 2009.

[21] P. J. Schreier and L. L. Scharf, "Second-order analysis of improper complex random vectors and process," *IEEE Trans. Signal Processing*, vol. 51, no. 3, pp. 714–725, 2003.

[22] B. Picinbono, "On circularity," *IEEE Trans. Signal Processing*, vol. 42, no. 12, pp. 3473–3482, 1994.

[23] E. Ollila, "On the circularity of a complex random variable," *IEEE Signal Processing Lett.*, vol. 15, pp. 841–844, 2008.

[24] B. Jelfs, D. P. Mandic, and S. C. Douglas, "An adaptive approach for the identification of improper complex signals," *Signal Processing*, vol. 92, no. 2, pp. 335–344, 2012.

[25] Y. Xia and D. P. Mandic, "Widely linear adaptive frequency estimation of unbalanced three-phase power systems," *IEEE Trans. Instrum. Meas.*, vol. 61, no. 1, pp. 74–83, 2012.

[26] S. C. Douglas and D. P. Mandic, "The least-mean-magnitude-phase algorithm with applications to communications systems," in *Proc. ICASSP*, 2011, pp. 4152–4155.

[27] A. Tarighat and A. H. Sayed, "Least mean-phase adaptive filters with application to communications systems," *IEEE Signal Processing Lett.*, vol. 11, no. 2, pp. 220–223, 2004.

[28] S. Javidi, S. L. Goh, M. Pedzisz, and D. P. Mandic, "The augmented complex least mean square algorithm with application to adaptive prediction problems," in *Proc. 1st IARP Workshop Cognitive Information Processing*, 2008, pp. 54–57.

[29] S. C. Douglas and D. P. Mandic, "Performance analysis of the conventional complex LMS and augmented complex LMS algorithms," in *Proc. IEEE Int. Conf. Acoustics, Speech, and Signal Processing*, 2010, pp. 3794–3797.

[30] Y. Xia and D. P. Mandic. (2011). Frequency estimation in smart grid in unbalanced system conditions. [Online]. Imperial College London, TR-021-11/2011. [Online]. Available: http://www.commsp.ee.ic.ac.uk/_mandic/research/smart-grid-and-renewables.htm

[SP]